Molecular Crystals and Liquid Crystals
Publication details, including instructions for authors and subscription information:
http://www.tandfonline.com/loi/gmcl20

Zinc Oxide Nanostructures by Solvothermal Synthesis

M. Segovia [a c], C. Sotomayor [d], G. González [b c] & E. Benavente [a c]

[a] Universidad Tecnológica Metropolitana, P.O. Box 9845, Santiago, Chile

[b] Universidad de Chile, P.O. Box 653, Santiago, Chile

[c] Center for the Development of Nanocience and Nanotechnology, CEDENNA, Santiago, Chile

[d] Catalan Institute of Nanotechnology (CIN2-CSIC) Campus Bellaterra—Edifici CM3 08193, Bellaterra, (Barcelona), SPAIN

Available online: 14 Feb 2012

To cite this article: M. Segovia, C. Sotomayor, G. González & E. Benavente (2012): Zinc Oxide Nanostructures by Solvothermal Synthesis, Molecular Crystals and Liquid Crystals, 555:1, 40-50

To link to this article: http://dx.doi.org/10.1080/15421406.2012.634363

Mol. Cryst. Liq. Cryst., Vol. 555: pp. 40–50, 2012

ISSN: 1542-1406 print/1563-5287 online
DOI: 10.1080/15421406.2012.634363

Taylor & Francis
Taylor & Francis Group

Zinc Oxide Nanostructures by Solvothermal Synthesis

M. SEGOVIA,[1,3] C. SOTOMAYOR,[4] G. GONZÁLEZ,[2,3] AND E. BENAVENTE[1,3,*]

[1]Universidad Tecnológica Metropolitana, P.O. Box 9845, Santiago, Chile
[2]Universidad de Chile, P.O. Box 653, Santiago, Chile
[3]Center for the Development of Nanocience and Nanotechnology, CEDENNA, Santiago, Chile
[4]Catalan Institute of Nanotechnology (CIN2-CSIC) Campus Bellaterra—Edifici CM3 08193 Bellaterra (Barcelona) SPAIN

The synthesis, characterization, and properties of three types of one-dimensional zinc oxide nanostructures are described. They were obtained by solvothermal treatment of nanometric zinc oxide as zinc ion source (i.e., starting from pure oxide), from a mixture of the oxide with stearic acid, and from intercalated oxide in the layered nanocomposite ZnO(stearic acid)$_{0.38}$. The reactions were performed at 180°C in a (1:1) ethanol/water mixture. Depending on the precursor and reaction times, morphologically homogenous phases corresponding to ZnO nanoneedles, nanorods or nanowires were obtained. Photoluminescence emissions were observed and are attributed to exciton transitions and to the presence of intrinsic defects such as oxygen and zinc interstitials. The band gap energies (Eg) were comparable to the values of bulk ZnO. The prepared nanostructures showed photocatalytic activities with respect to the degradation of methylene blue which were comparable to that of bulk zinc oxide.

Keywords Intercalation; nanostructure; photocatalysis; zinc oxide

Introduction

Zinc oxide, ZnO, is a semiconductor which has attracted considerable attention over the last few years due to its numerous attractive properties. It is actually considered, within the new-generation semiconductor materials, as one of the most important, having great potential for applications in optoelectronics, sensors, field emission, light-emitting diodes and photocatalysis [1]. Most research on ZnO-based materials performed during the last few years has been focused on the development of different synthetic routes for obtaining nanostructured blocks, for instance nanowires, nanorods, nanobelts or nanoribbons, especially in terms of controlling their size, shape, morphological homogeneity and its ability to form hierarchical architectures [2–5].

In this context, a variety of physical and chemical methods have been employed. Among the physical methods most are vapour-solid processes like [6] thermal reduction [7], pyrolysis [8], vapour-liquid-solid (VLS) growth [9], chemical vapour deposition (CVD)

*Address correspondence to E. Benavente, Universidad Tecnológica Metropolitana, P.O. Box 9845, Santiago, Chile. E-mail: ebenaven@utem.cl

[10], metal organic CVD (MOCVD) [11], and molecular beam epitaxy [12], often utilizing metals as catalysts. In these procedures, after initial nucleation or incubation, the crystallites develop into three dimensional structures with well-defined crystallographic faces [13]. However these in general methods require high temperatures and sophisticated instruments.

Wet chemistry techniques using chemical approaches such as precipitation, sol-gel, and solvothermal processes are usually simpler and proved to be very effective for large scale production. The solvothermal techniques have been widely applied for preparing a number of different ZnO nanostructures generally by autoclaving at temperatures between 100 and 200°C alkaline zinc salts solutions in alcoholic media often in the presence of different additives and/or reaction conditions. Liu et al. [14], for instance, obtained monodispersed, highly crystalline ZnO nanorods by adding ethylene diamine to the reaction mixtures. Cheng et al. [15] demonstrated the importance of alcohol (methanol or ethanol) in the preparation of one-dimensional ZnO nanostructures, by producing them directly by autoclaving zinc acetylacetonate and sodium hydroxide in an alcoholic medium without any other additive. In methanol, the resulting rods had diameters of about 25 nm and a length of about 100 nm. The use of an aqueous medium often induces more complex reactions leading not only to different morphologies but also towards generating arrays and hierarchical architectures. This occurs, for instance, in some hydrothermal reactions using cetyltrimethylammonium bromide (CTAB) as additive.

As reported by Li et al. [16], hydrothermal heating at 130°C of an alkaline solution of zinc acetate with CTAB leads to arrays of nanorods in the form of flower-like structures formed by tapered ZnO nanorods with diameter decreasing from about 400 nm at the base, to about 80 nm at the top. However the same reaction conducted at 150–180°C produces cabbage-like ZnO structures, built up by overlapping bi-dimensional ZnO nanosheets. More recently Qiu et al. [17] reported that the hydrothermal treatment of zinc acetate and urea in the presence of CTAB leads to superstructures of meso/micro-porous ZnO nanoplates. However this product appears to be a nanocomposite of hydrozincite with CTAB which may be converted into porous single-crystalline ZnO nanoplates by calcination at 400°C.

The variety of morphologies of ZnO nanostructures, obtainable by controlling the solvothermal reaction conditions, is mainly due to different surfaces structures of wurzite ZnO having different growth rates what could induce anisotropic growth [13]. Wurzite ZnO is a polar crystal formed by alternately stacking crystal planes [0001] and [000-1], charged positively (Zn^{2+}) and negatively (O^{2-}) respectively, along the c-axis [18]. The highest growth rate on ZnO crystallites is along the c-axis, through the positively charged crystal plane. Accordingly and also agreeing with most of reported procedures, alkaline solutions rich in $(ZnO_2)^{2-}$ species are especially appropriate for producing 1D ZnO nanostructures solvothermally. However, preferential growth along other directions may also be attained by regulating, for instance, the nature and/or activity of crystallization nutrients or by means of additives for diminishing or suppressing growth along the 0001 plane [19]. Among the variables involved in morphological equilibriums in these preparations, the zinc-ions source should be also considered.

Most solvothermal procedures for preparing ZnO nanostructures do consider, as a first step, the formation of crystallites, generally starting from common soluble salts. To the best of our knowledge, any attempts to convert directly the solid oxide into nanostructured products have been yet not reported. Preliminary tests showed that commercial zinc oxide remains practically unaltered after normal solvothermal treatments; however we realized that nanometric particles of the oxide, freshly prepared in the lab by conventional reaction of a zinc salt with alkali, may be directly converted into nanostructured products. In this work we describe the solvothermal conversion of nanometric ZnO particles into a

morphologically homogeneous phase of nanoneedles. We compare this with results observed from autoclaving of both, the same oxide, but using stearic acid as additive, and the layered nanocomposite ZnO(stearic acid)$_{0.38}$, where the formation of nanorods and nanowires respectively, was attained.

Experimental

Synthesis

All the chemical reagents used in the experiments were obtained from commercial sources as guaranteed-grade reagents. $ZnSO_4$, NaOH and Na_2CO_3 were purchased from Merck and stearic acid purchased from Aldrich. The analytical grade solvents were used as received and nanopure water was used throughout.

Precursor Solution Preparation

ZnO. The typical synthetic procedure to prepare ZnO was as follows: 10 ml of $ZnSO_4$ (1 M) solution was mixed with 10 ml Na_2CO_3 (1 M) /NaOH (1 M) (1:1) at temperature of 60°C under vigorous stirring which resulted in formation of a white suspension. The suspension was then separated with a centrifuge and washed three times with distilled water.

Solvothermal Method

ZnO needles. 0.5 g of *ZnO* was suspended in a mixture of 4.5 ml water-ethanol (1:1). The suspension was transferred to a Teflon vessel in stainless steel autoclave. The reaction was held for 72 hours at 180°C. The product obtained is separated by centrifugation, washed with ethanol and dried in an oven for 12 hours at 70°C.

ZnO nanorods. 0.25 g of *ZnO* and 0.25 g stearic acid are suspended in a water-ethanol mixture (1:1) 4.5 ml. The suspension was transferred to a Teflon vessel in stainless steel autoclave. The reaction was held for 168 hours at 180°C. The product obtained is separated by centrifugation, washed with ethanol and dried in an oven for 12 hours at 70°C.

ZnO nanowires. 0.5 g of layered nanocomposite ZnO(stearic acid)$_{0.38}$ was suspended in a water-ethanol mixture (1:1) 4.5 ml. The suspension was transferred to a Teflon vessel in stainless steel autoclave. The reaction was held for 168 hours at 180°C. The product obtained is separated by centrifugation, washed with ethanol and dried in an oven for 12 hours at 70°C.

Product Characterization

Products were characterized by chemical analysis (SISONS ES-1108), X-ray Diffraction Analysis (DRX, SIEMENS D-5000, Cu-Kα radiation), Fourier Transform Infrared Spectroscopy (FT-IR, BRUKER Vector 22) and Scanning Electron Microscopy (SEM EVO MA 10 ZEISS)

Optical Measurements

The diffuse reflectance UV–vis spectra were recorded in the range 200–800 nm, at medium scan rate and slit 0.1 nm at room temperature, using a Shimadzu UV–vis spectrophotometer,

model 2450 PC equipped with an integrating sphere. Barium sulphate was used in all cases as reference material. Reflectance measurements were converted to absorption spectra using the Kubelka-Munk function. Photoluminescence (PL) spectra of solid samples were recorded at room temperature with a Perkin Elmer Model L55 spectrofluorometer. The spectra were obtained under similar conditions, using an excitation wavelength of 315 nm.

Photocatalytic Properties

The photocatalytic activity of the products was evaluated by measuring the degradation of methylene blue (MB) in water under UV illumination (mercury lamp 300W), monitoring the MB concentration from its absorption spectrum recorded with a UV-visible spectrometer (Shimadzu UV-2450) with the sample in a liquid cuvette using nanopure water as reference. Methylene blue was employed in a concentration of 2×10^{-5} M. In a typical experiment, 2.5×10^{-3} g of nanostructures with 50 mL of dye solution was transferred into the reaction container. Samples were extracted every 30 min under uninterrupted irradiation. A water cooling jacket in the reactor kept the temperature constant (25°C) during irradiation. The degradation of methylene blue was monitored by measuring its absorbance in the solution at 665 nm using the UV–vis spectrophotometer.

Results and Discussion

As detailed in the section above, the ZnO used for performing the experiment described here was obtained from drying the hydrogel generated by hydrolysing zinc nitrate in alkaline medium. As observed in the difractogramm reproduced in Fig. 1a, the product corresponds to ZnO wurtzite phase (card JCPDS 36-1451). Estimation of particle size using the Scherrer formula [20] approach indicates an average grain diameter of 27 nm. As expected, the suspension of this product in a mixture ethanol/water, as prepared for the thermal treatment, is slightly alkaline (pH 8). A series of experiments were performed in order to optimize the products taking the morphological homogeneity of resulting phases as quality criterion. In general these, as well as the experiments discussed below, are positively influenced by higher temperatures. The higher the temperature is, the greater the degree of conversion of the precursor into tubular nanostructures. Therefore all experiments were performed at 180°C. Concerning the reaction time reported for the treatment of the pure oxide, best results were obtained after 72 h heating. Shorter times lead to a mixture of morphologically different phases, among which particles and rod-shaped species could be distinguished. Larger heating times produce mixed phases, in which, together with other types of nanostructures, ZnO nanotubes were also observed. Figure 2 illustrates a SEM image of the product obtained from the solvothermal treatment, 72 h at 180°, of a suspension of the ZnO nanoparticles in alcohol/water (1:1). There, it may be clearly seen a rather homogeneous phase constituted pyramid, like-rods with diameters (d) in the range of 450–900 nm and lengths (l) between 8 and 20 microns which we have classified as nanoneedles. This corresponds to an aspect ratio (d/l) of about 0.01.

It is interesting to remark that in these experiments, availability of crystallization nutrients should necessarily arise only from the re-dissolution of the oxide itself, and from the corresponding variations in hydrolysis equilibriums. At least two stages, probably simultaneous, should occur, the generation of zinc species in the solution of the precursor and the anisotropic growing of the new nanostructure. In order to get a better understanding of the variables involved in these processes two further reactions were investigated: The same process but in presence of stearic acid as additive and the thermal treatment of the

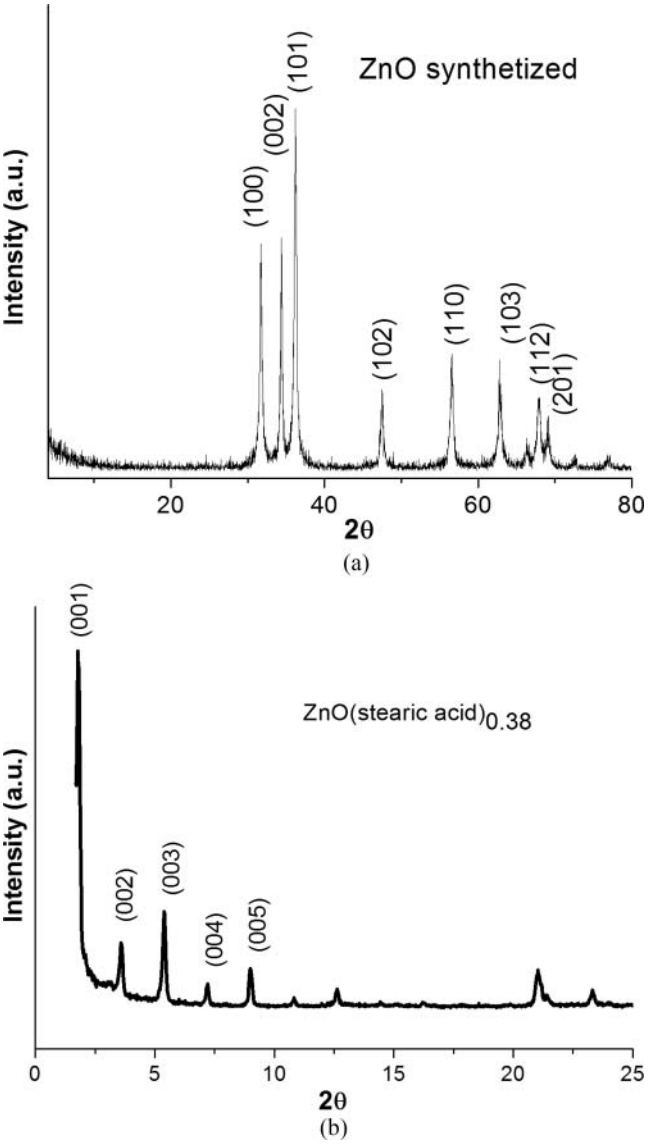

Figure 1. Powder X-ray diffraction patterns; (a) ZnO, (b) layered nanocomposite ZnO(steric acid)$_{0.38}$

nanocomposite ZnO(stearic acid)$_{0.38}$ (Fig. 1b) both performed under the same conditions except reaction time than those already commented above for the oxide alone. X-Ray diffraction patterns of the products obtained from solvothermal treatment of ZnO in the presence of stearic acid and of the layered nanocomposite ZnO/Stearic acid are shown in Fig. 3. As observed, both are similar to that of the pristine oxide (Fig. 1), indicating that all of them are in a wurzite phase. All the peaks may be well indexed to hexagonal ZnO agreeing with the reported ones, (card JCPDS 36-1451). It should be noted that, not only the position of diffraction peaks, but also the relative intensities of the patterns matched accurately. The intensity of the diffraction peak corresponding to the (002) plane

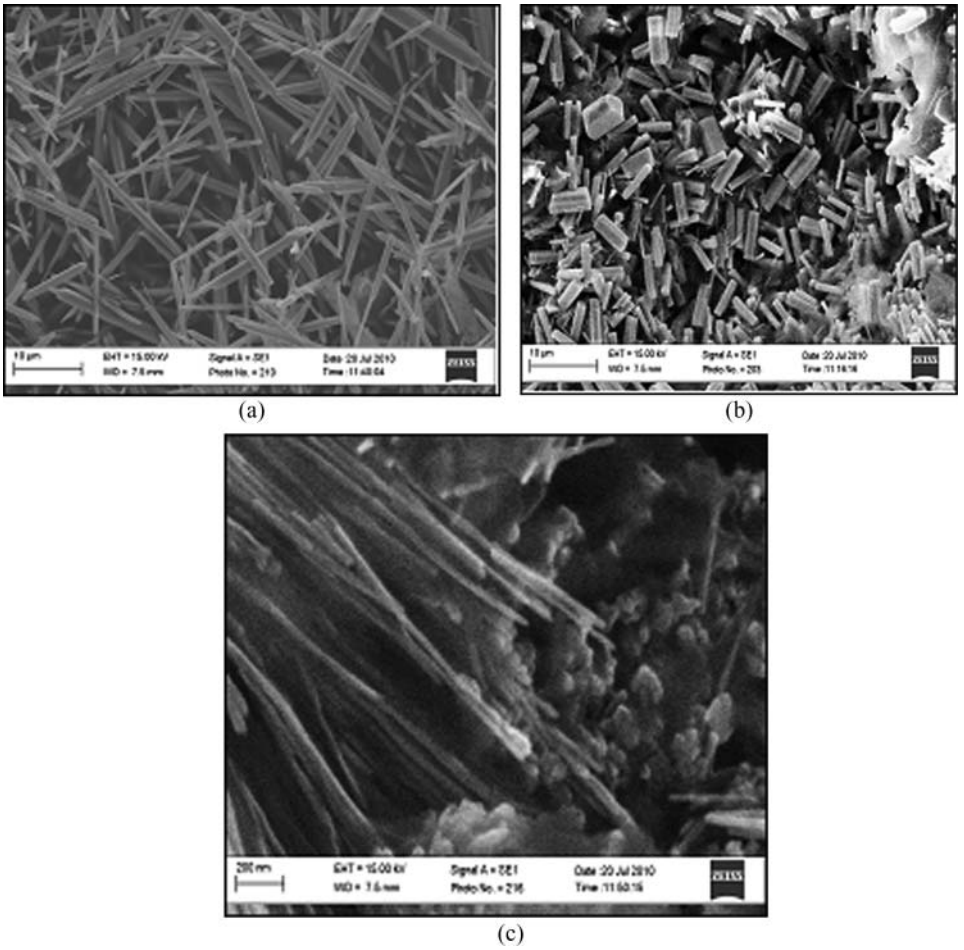

Figure 2. SEM images of the nanostructures; (a) nanoneedles, (b) nanorods and (c) nanowires.

is observed to be higher, indicative of a growth of the ZnO nanostructures highly oriented. As observed in the SEM images illustrated in Fig. 2 together with Fig. 3 above and data in Table 1, all three products described in this work may be roughly classifies as one-dimensional nanostructures; however they present different morphologies. Indeed, the reaction performed in presence of the fatty acid leads to the formation of rods, almost vertically aligned to each other, and possessing diameters in the range of 40–160 nm and a length of a few microns. Meanwhile the nanocomposite ZnO/Stearic acid leads to the formation of nanowires with diameters in the range 30–50 nm and lengths between 800 and 1000 nm.

It is interesting to compare the different shapes of the nanostructures arising from the reactions above. The average aspect ratio of about 0.05 in needles obtained from pure oxide, decreases to about 0.01 in the nanorods obtained in the presence of stearic acid. This clearly indicates that the fatty acid causes a more marked preferential c-axial growth thus leading to the rods. Nanoneedles display, in turn, absolute dimensions length and width notably much larger. Considering the size of the ZnO precursor particles (about 30 nm)

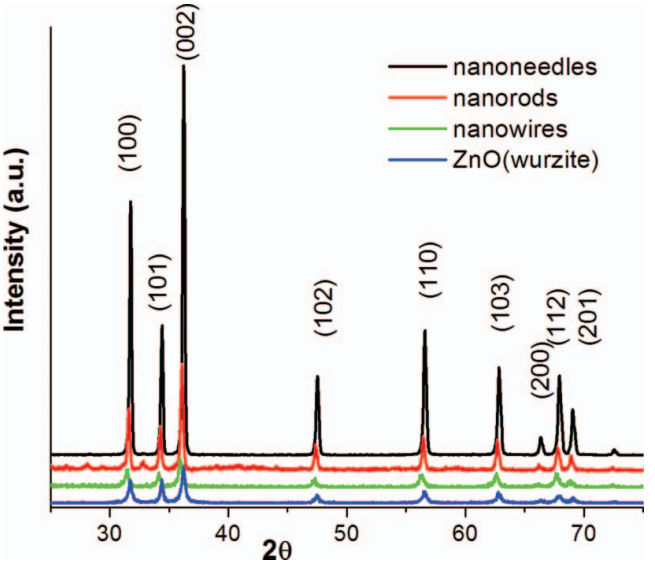

Figure 3. Powder X-ray diffraction patterns of the nanostructures.

the resulting structure responds mainly to a kind of agglomeration/melting process. That notwithstanding, in this process the growth rate along the (0001) polar direction is still relatively high. Concerning the rods, there are at least two variables which permit one to understand the enhanced tendency to grow along the c-axis, observed in the presence of the fatty acid. One of them is the lower pH in the presence of a carboxylic acid. This on one hand could induce a higher solubility of pristine oxide nanoparticles, thus increasing the activity of zinc species in the solution. And on the other hand, it could partially remove the OH^- layer from the [0001] crystal surface, thus increasing the surface energy on the [0001] facet, in this way positively affecting the kinetics of nucleation and the accumulation of zinc species in growth front [21]. A second factor could be the coordination properties of the carboxylate group, which could also favour the dissolution of the precursor and, simultaneously, the transport to and deposition of zinc species upon the [0001] crystal plane charged positively, by reducing the positive charge on zinc ions. In the case of the nanowires obtained from the ZnO/stearic acid nanocomposite we are comparatively in

Table 1. Precursor and products obtained for solvotermal method

	Solvothermal method *Reaction Conditions*			Product *Shape and Size*		
Precursor	T°C	Time (h)	Shape	Diameter (nm)	Length (μm)	Aspect ratio (d/l)
ZnO Nanoparticles	180	72	nanoneedles	450–900	8–20	0.05
ZnO Nanoparticles + Stearic acid	180	168	nanorods	40–160	5–8	0.014
$ZnO(stearic\ acid)_{0.4}$	180	168	nanowires	30–50	~0.8–1	0.04

an opposite situation; the aspect ratio is the same than for the needles but the diameters are about 10 and 100 times shorter than the rods and the needles respectively. Moreover, pH is expected to remain nearly neutral during the process. Apparently, in this case 1D nanostructures formation follows a different mechanism. In this case we think that here could be a rolling up process, like that observed in the conversion of laminar V_2O_5/amine nanocomposites into nanotubes [22], but followed by surfactant segregation as the one observed in the conversion of V_2O_5/thiol nanocomposites into nanocogs [23].

Photoluminescence (PL) of the hydrothermally synthesized nanostructures was observed at room temperature. Figure 4a shows PL spectra of the ZnO nanostructues recorded with an excitation wavelength of 315 nm. The visible emission is usually considered to be related to various intrinsic defects, these defects are located at the surface of the ZnO structure [24]. In general, a strong emission peak located at 385 nm, corresponds to the band gap of bulk ZnO, and several weak blue emission peaks at 420, 462, 480 nm are attributed to the exciton transitions and to the presence of intrinsic defects such as oxygen and/or zinc interstitial atoms. Green emissions at 570 nm are attributed to the recombination of a photo-generated hole with an electron that belongs to a singly ionized oxygen vacancy. In the curves of the nanoneedles and nanowires the emission diminishes probably due to a greater contribution of defects [25].

Figure 4b reproduces the diffuse reflectance spectra, after a Kubelka–Munk transformation, of series of the products obtained during this study, comparing them with that of pristine ZnO. They show broad and strong absorptions in the ultraviolet region near the visible light region, which is characteristic of ZnO wide-band-gap semiconductor materials [26]. Although the shape of spectra is in general the same, the spectra were shifted depending of the nanostructures. Nanorods structures exhibited absorption bands slightly red shifted relative to the absorption bands of other nanostructures, indicating that the density of defects in the nanoneedles and nanowires is higher than in the nanorods [27]. An evaluation of the optical gap in the different products was made using the plots $(K/Sh)^2$ versus energy

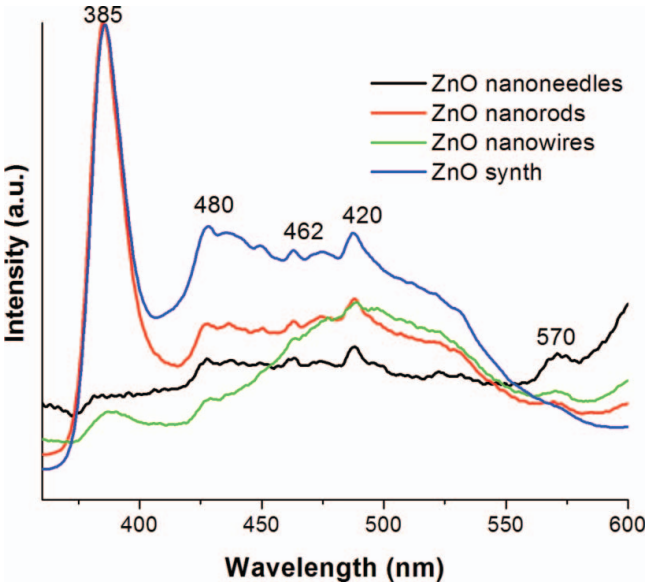

Figure 4a. Photoluminescence spectra of the nanostructures.

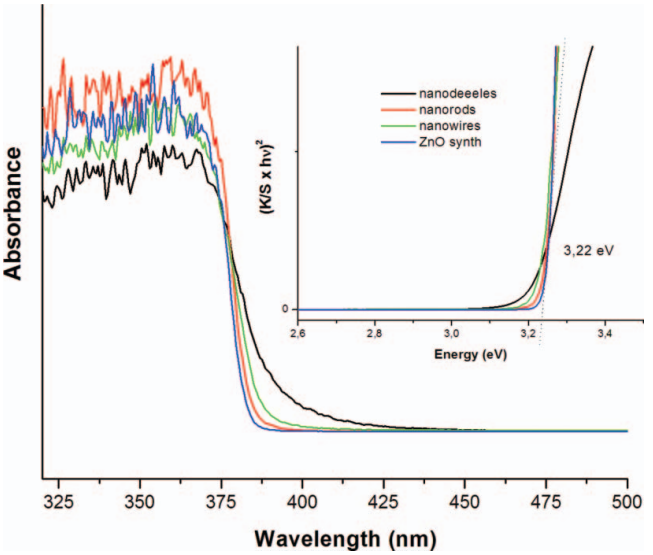

Figure 4b. UV-visible absorption spectra of the nanostructures, Inset: Band gap energy (*E*g) of the samples.

displayed in the inset of Fig. 4b, the band gap values observed for all nanostructures were similar, independently of their morphology.

The photocatalytic activity of these ZnO nanostructures was investigated by evaluating the degradation of methylene blue. The spectrum in Figure 5 shows the degradation of dye as a function of time. We observed an average decomposition for all the samples of more than 80% in 400 min.

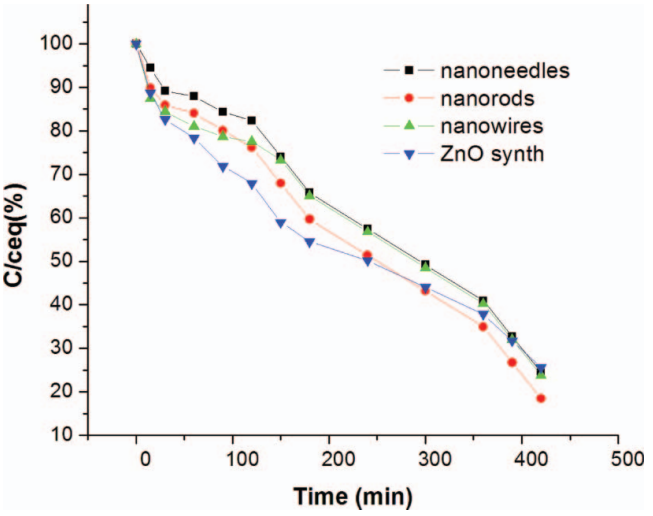

Figure 5. Photodegradation of methylene blue using ZnO shyntetized and nanostructures.

Conclusions

In contrast to commercial available zinc oxide particles, zinc oxide nanoparticles prepared from zinc salts in alkaline medium can be solvothermally converted into one-dimensional nanostructures without any further additive. The process appears to occur via an agglomeration/melting mechanism and leads to nanoneedles of relatively large dimensions. In the presence of stearic acid the same reaction produces nanorods. A lower pH in the medium and a possible interaction of the carboxylic acid with the [0001] crystal plane surface appears to be responsible for the relatively lower aspect ratio (d/l) observed in the presence of this additive.

The use of the layered hybrid nanocomposite ZnO/stearic acid as zinc source instead the mixture ZnO-fatty acid as above, but using the same reaction conditions, leads to the formation of ZnO nanowires. In this case, the formation mechanism of one-dimensional nanostructures does appear to be related more to a rolling-up/surfactant-segregation process than with the characteristic ZnO crystallites growth.

Independently of preparation conditions, all three nanostructured products described here have a hexagonal wurtzite structure. Accordingly the electronic structure of the products, as deduced from their UV-visible absorption and emission spectra as well as from their photocatalytic ability, is in all the cases similar. Confinement effects, evaluated by measuring optical band gaps, also appear to be similar in the precursor and in the products. Additional experiments, necessary for evaluating the actual potential of the synthesis approach described here for designing and preparing zinc oxide nanostructures, are in progress.

Acknowledgments

Research partially financed by FONDECYT (Contracts 1090282, 1111029) Basal Financing Program CONICYT, FB0807 (CEDENNA), Millennium Science Nucleus P10-061-F.

References

[1] Wang, Z. L. (2008). *ACS Nano*, *2*, 1987.
[2] Jiang, P., Zhou, J. J., Fang, H. F., Wang, C. Y., Wang, Z. L., & Xie, S. S. (2007). *Adv. Funct. Mater.*, *17*, 1303.
[3] Sounart, T. L., Liu, J., Voigt, J. A., Hsu, J. W. P., Spoerke, E. D., Tian, Z., & Jiang Y. (2006). *Adv. Funct. Mater.*, *16*, 335.
[4] Hsu, J. W. P., Tian, Z. R., Simmons, N. C., Matzke, C. M.,Voigt, J. A., & Liu, J. (2005). *Nano Lett.*, *5*, 83.
[5] Stroyuk, O. L., Dzhagan, V. M., Shvalagin, V. V., & Kuchmiy, S. Y. (2010). *J. Phys. Chem. C.*, *114*, 220.
[6] Wu, Y., & Yang, P. (2001). *J. Am. Chem. Soc.*, *123*, 3165.
[7] Park, W. I., Yi, G. C., Kim, M., & Pennycook, S. J. (2002). *Adv. Mater.*, *24*, 1841.
[8] Krunks, M., & Mellikov, E. (1995). *Thin Solid Films*, *270*, 33.
[9] Pan, Z. W, Dai, Z. R., & Wang, Z. L. (2001). *Science*, *291*, 1947.
[10] Satoh, Y., Ohshio, S., & Saitoh, H. (2005). *Sci. Technol. Adv. Mater.*, *6*, 215.
[11] Yasuda, T., & Segawa, Y. (2004). *Phys. Status Solidi. b.*, *241*, 676.
[12] El-Shaer, A., Mofor, A. C., Bakin, A., Kreye, M., & Waag, A. (2005). *Superlatt. Microstruct*, *38*, 265.
[13] Wang, Z. L. (2004). *J. Phys. Condens. Matter.*, *16*, R829.
[14] Liu, B., & Zeng, H. C. (2003). *J. Am. Chem. Soc.*, *125*, 4430.
[15] Chen, D., Jiao, X., & Cheng, G. (2000). *Solid State Commun.*, *113*, 363.

[16] Li, F., Hu, L., Li, Z., & Huang, X. (2008). *J. Alloys Compd.*, *465*, L14.
[17] Qiu, Y., Chen, W., & Yang, S. (2010). *J. Mater. Chem.*, *20*, 1001.
[18] Wang, Z. L., Kong, X. Y., & Zou, J. M. (2003). *Phys. Rev. Lett.*, *91*, 185502.
[19] Zhang, X. L., Qiao, R., Qiu, R., Kim, J. C., & Kang, Y. S. (2009). *Cryst. Growth Des.*, *9*, 2906.
[20] Patterson, A. L. (1939). *Phys. Rev.*, *56*, 978.
[21] Baruah, S., & Dutta, J. (2009). *Sci. Technol. Adv. Mater.*, *10*, 013001.
[22] O'Dwyer, C., Navas, D., Lavayen, V., Benavente, E., Santa Ana, M. A., Gonzalez, G., Newcomb, S. B., & Sotomayor, C. M. (2006). *Chem. Mater.*, *18*, 3016.
[23] O'Dwyer, C., Lavayen, V., Fuenzalida, D., Newcomb, S. B., Santa Ana, M. A., Benavente, E., González, G., & Sotomayor, C. (2007). *Phys. Stat. Sol. B.*, *244*, 4157.
[24] Li, Y., Feng, H., Zhang, N., & Liu, C. (2009). *Mater. Sci. Poland*, *27*, 551.
[25] Singh, A. K., Viswanath, V., & Janu, V. C. (2009). *J. Luminescence*, *129*, 874.
[26] Cho, S., Jang, J. W., Lee, J. S., & Lee, K. H. (2010). *Langmuir*, *26*, 14255.
[27] Lee, J., & Yoon, M. (2009). *J. Phys. Chem. C*, *113*, 11952.